LAWRENCE
LIVERMORE
NATIONAL
LABORATORY

UCRL-TR-216377

# Remote Sensing of Alpha and Beta Sources - Modeling Summary

J. Dignon, M. Frank, N. Cherepy

October 20, 2005

This work was performed under the auspices of the U.S. Department of Energy by University of California, Lawrence Livermore National Laboratory under Contract W-7405-Eng-48.

**Remote Sensing of Alpha and Beta Sources – Modeling Summary**

**J. Dignon, M. Frank, and N. Cherepy**

Evaluating the potential for optical detection of the products of interactions of energetic electrons or other particles with the background atmosphere depends on predictions of change in atmospheric concentrations of species which would generate detectable spectral signals within the range of observation. The solar blind region of the spectrum, in the ultra violet, would be the logical band for outdoor detection (see Figure 1). The chemistry relevant to these processes is composed of ion-molecule reactions involving the initially created $N_2^+$ and $O_2^+$ ions, and their subsequent interactions with ambient trace atmospheric constituents.

Effective modeling of the atmospheric chemical system acted upon by energetic particles requires knowledge of the dominant mechanism that exchange charge and associate it with atmospheric constituents, kinetic parameters of the individual processes (see e.g. Brasseur and Solomon, 1995), and a solver for the coupled differential equations that is accurate for the very stiff set of time constants involved. The LLNL box model, VOLVO , simulates the diel cycle of trace constituent photochemistry for any point on the globe over the wide range of time scales present using a stiff Gear-type ODE solver, i.e. LSODE. It has been applied to problems such as tropospheric and stratospheric nitrogen oxides, stratospheric ozone production and loss, and tropospheric hydrocarbon oxidation. For this study we have included the appropriate ion flux.

The LLNL box model can flexibly accommodate a large number of chemical species and thermal and photolytic reactions. Here we have included 103 chemical species and a chemical mechanism consisting of over 200 reactions. Code for the specific photochemical mechanisms is produced by a code generator with human modeler-friendly inputs and interface, with flexible start times (midnight, noon or other). Photolysis frequencies are updated (using a lookup-table module) on the variable time

step of the solver. Overhead ozone abundance and temperature can be climatological or retrieved from other model simulations. Output times are flexible and user-defined.

For this study the box chemistry model has constant temperature and pressure, with initial conditions taken from our existing higher dimensional atmospheric model (Rotman, et al, 2004). Physical and constituent variables can also be modeler-specified. We have utilized this feature in order to vary the flux of ion pairs entering the system. Initial conditions and can incorporate terms representing transport, deposition, and/or emissions. In the studies presented in this paper, the model did not include diffusion into or out of the irradiated volume nor did it include surface emissions or deposition that may be present in an in situ environment. The model can be run at all locations on the globe for any season.

In our first modeling experiment we have prescribed the surface pressure at an ambient temperature of 300K and a relative humidity of roughly 100 percent. The incoming solar radiation for photolysis is representative of noon at low latitudes. There is an ionizing radiation flux of 1.05x10^9 ion pairs per cm3. The computed concentrations of select species with respect to time are shown in Figure 2a and b. Figure 2a illustrates the effect of ionizing radiation on the abundances of select nitrogen, oxygen and hydrogen species, while Figure 2b shows the photochemistry under the same atmospheric conditions without ionizing radiation. Comparison shows that there is a significant effect on nitrogen, oxygen and hydrogen containing species when ionizing radiation is added, with the concentrations of most species changing by at least one order of magnitude. The major species showing largest increases in concentration in the solar blind region are HNO3, NO2, and N2O5. This will be discussed further below.

Moss et al (1999) have performed a similar study using an ion chemistry model developed for the mesosphere. They include ionic and stable species of nitrogen oxygen and hydrogen only. Where possible we have chosen similar physical parameters in this experiment. Our results are not expected to mirror those of Moss et al (1999), because we are starting our model runs with typical background concentrations of many more chemical species, and an ion background of zero. This model uses a chemical mechanism appropriate to the actual outside air at the surface. The LLNL model includes hydrocarbons, bromine and chlorine species, all of which the hydrogen oxygen and

nitrogen species react. As stated above, we initialize the concentrations of all species according to monthly average background concentrations. It is not clear what initial concentrations used in the Moss et al (1999)work. Our model assumes, according to Brasseur and Solomon (1995), that due to their relatively high concentrations in the atmosphere, all of the ionization occurs on N2 and O2 molecules. The relative fractions of dissociative ionization are .185 and .076 respectively.

If one compares the results, of our Figure 2a to Figure 1 of Moss et al (1999) we see that the LLNL we have only run our experiment for 1 day (order 10^4 seconds. Moss et al (1999) have run their simulation to 10^6 seconds). The change in concentrations of species show similar trends. The ozone concentration determined in this model study appears to be similar to Moss et al. (1999). The O3 concentration increases by roughly 1 order of magnitude and then decreases then quasi equilibrium has been achieved. Unlike Moss et al., our simulation shows little change in the N2O concentration. This result is expected since N2O has a relatively high background concentration, and a very long time constant in the troposphere making it virtually chemically inert near the surface. Like Moss et al (1999) our HNO3 concentration increases by several orders of magnitude. One notable difference between the two studies is the response of the species H2O2. This study shows a steady decrease in the H2O2 concentration, whereas the Moss study starts at a much lower initial concentration, increase and then decreases. The difference in final concentrations is significant. This is most likely due to differences in initial concentrations, the kinetic reaction rates used, and differences in the chemical mechanisms between the models.

The solar blind region, shown in Figure1, would be the logical region for remote detection. Nitric Acid, N2O5, and NO2 and NO being the most prominently observed products, would be the prime candidates of spectral bands for measurement purposes. Absorption bands of N2O5 and HNO3 in the region where NO fluoresces will decrease any available uv signal in the solar blind region.

In a second model experiment we compared the influence of air pollution on the detectablity of ionization. In these runs the model was initialized by our 3-dimensional model (Rotman, et al 2004) for two locations one representative of a clean air remote site the second a polluted urban site. Figures 3a and b show simulations for the clean air site.

Figure 3a represents the atmospheric concentrations with ionizing radiation, while Figure 3b includes no ionization. Figure 4a and b are representative of a polluted regime with and without ionization respectively. These runs were performed using the diel cycle whereas the previous experiment was performed with constant sunlight. The affect of varying sunlight is small compared to the ionization effect. When comparing these simulations it is clear to determine that the effect of ionizing radiation is the dominant process in both regimes.

Figures 5 and 6 represent the results of our third model experiment. They illustrate the concentration of species after 5 hours at various distances up to 3 cm from an alpha radiation source and up to 12 cm for a beta source respectively. Figures 5a, b, and c show values for 0.1, 1.0 and 100 microCi Po210 alpha source while Figures 6a, b and c represent the same for a 0.1, 1.0 and 100 microCi Sr90 beta source out to 10 cm. When comparing figures 5a, b, and c it can be seen that the trends in concentration with distance from the sources are of similar shape. The magnitude and radial distances from the source where changes from the initial conditions are detected increase with increasing activity as expected. The same can be said regarding the beta source in Figures 6. Results here suggest source strengths of less than 0.1 microCi Po210 alpha source and less than 1.0 microCi Sr90 beta source are unlikely to be distinguished from the background by a remote sensing method.

The concluding results of this model study suggest that detecting radiation through remote uv detection under normal atmospheric conditions is unlikely to be successful.

*References:*

Brasseur G and S Solomon, *Aeronomy of the Middle Atmosphere,* Reidel Publishing Co, Boston, 1995.

Moss C., R Geller, D. Miligan, J. Valencia, J. Zinn, Remote sensing of Radiation, *Nuclear Instruments and Methods in Physics Research A,* **422,** 1999.

Rotman, D., Rotman, D.A., C.S. Atherton, D.J. Bergmann, P.J. Cameron-Smith, C.C. Chuang, P.S.Connell, J.E. Dignon, A. Franz, K.E. Grant, D.E. Kinnison, C.R. Molenkamp, D.D. Proctor, J.R. Tannahill, IMPACT, the LLNL 3-D global atmospheric chemical transport model for the combined troposphere and stratosphere: Model description and analysis of ozone and other trace gases, *J. Geophys. Res.*, 2004.

Figure1. Solar spectrum with NO and N2 Absorption and Fluorescence bands.

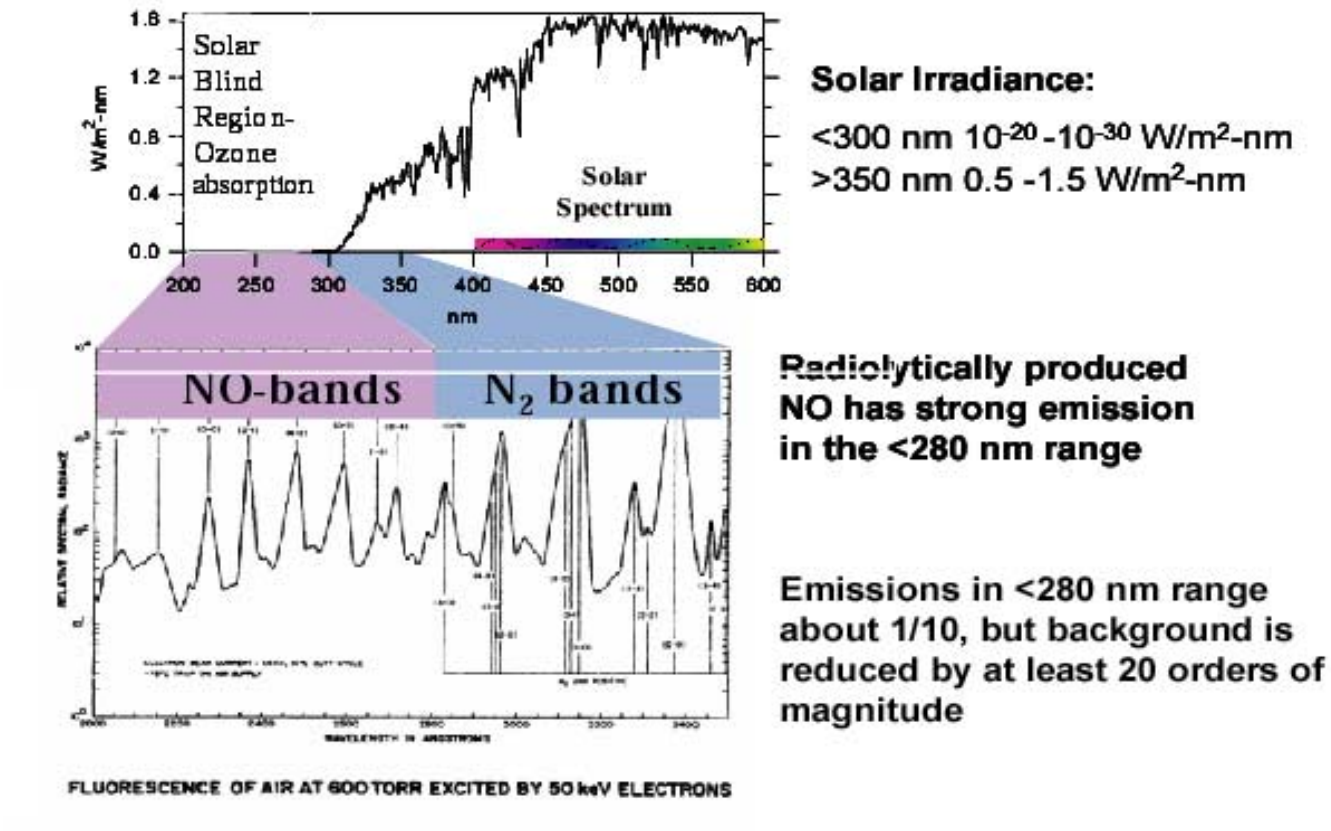

Figure 2. Molecular species concentrations (mole fraction vs. seconds). [a] with 1.05e9 ion pairs /cm^3 flux. [b] without ionization.

[a]

[b]

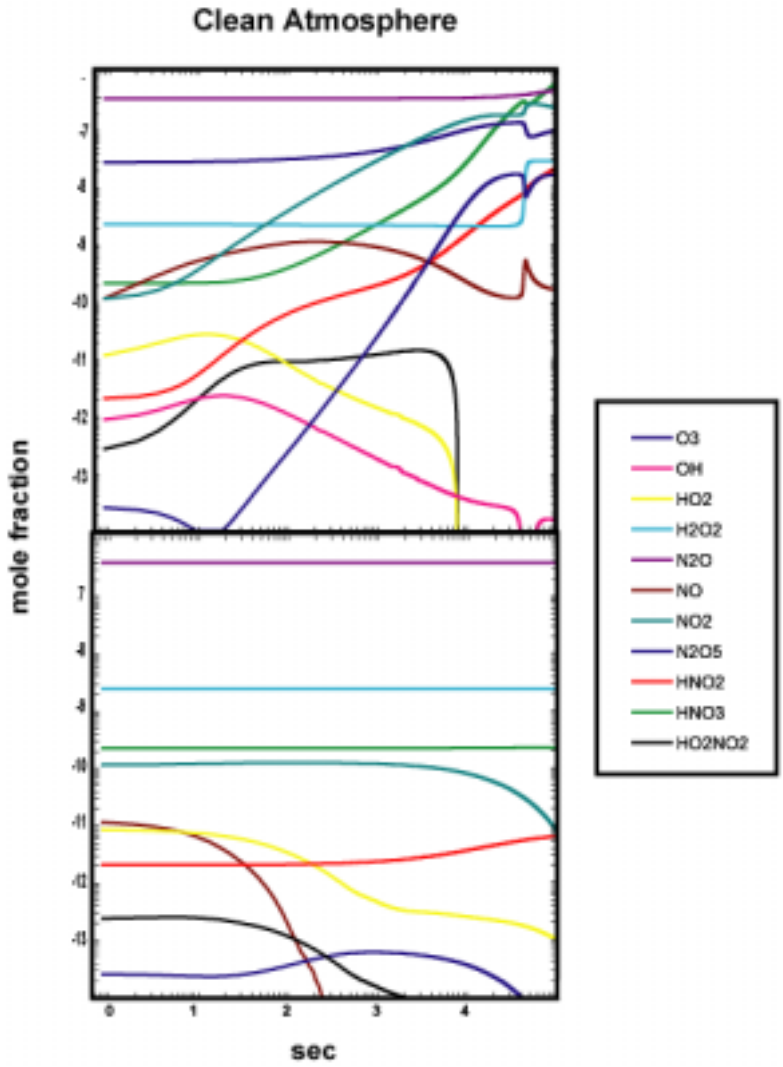

Figure 3. Molecular species concentrations (mole fraction vs. seconds)in a clean background regime, full solar cycle. [a] with ionizing radition [b] without ionization

[a]

[b]

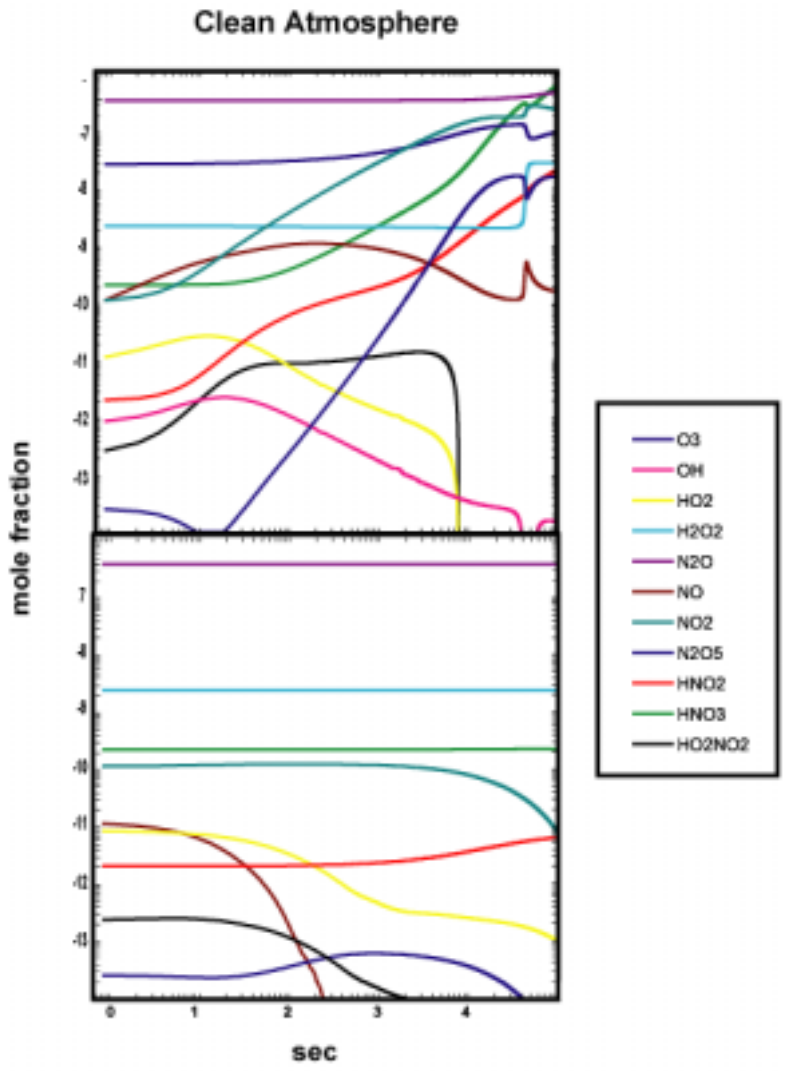

Figure 4. Molecular species concentrations (mole fraction vs. seconds)in a polluted background regime, full solar cycle. [a] with ionizing radition [b] without ionization

[a]

[b]

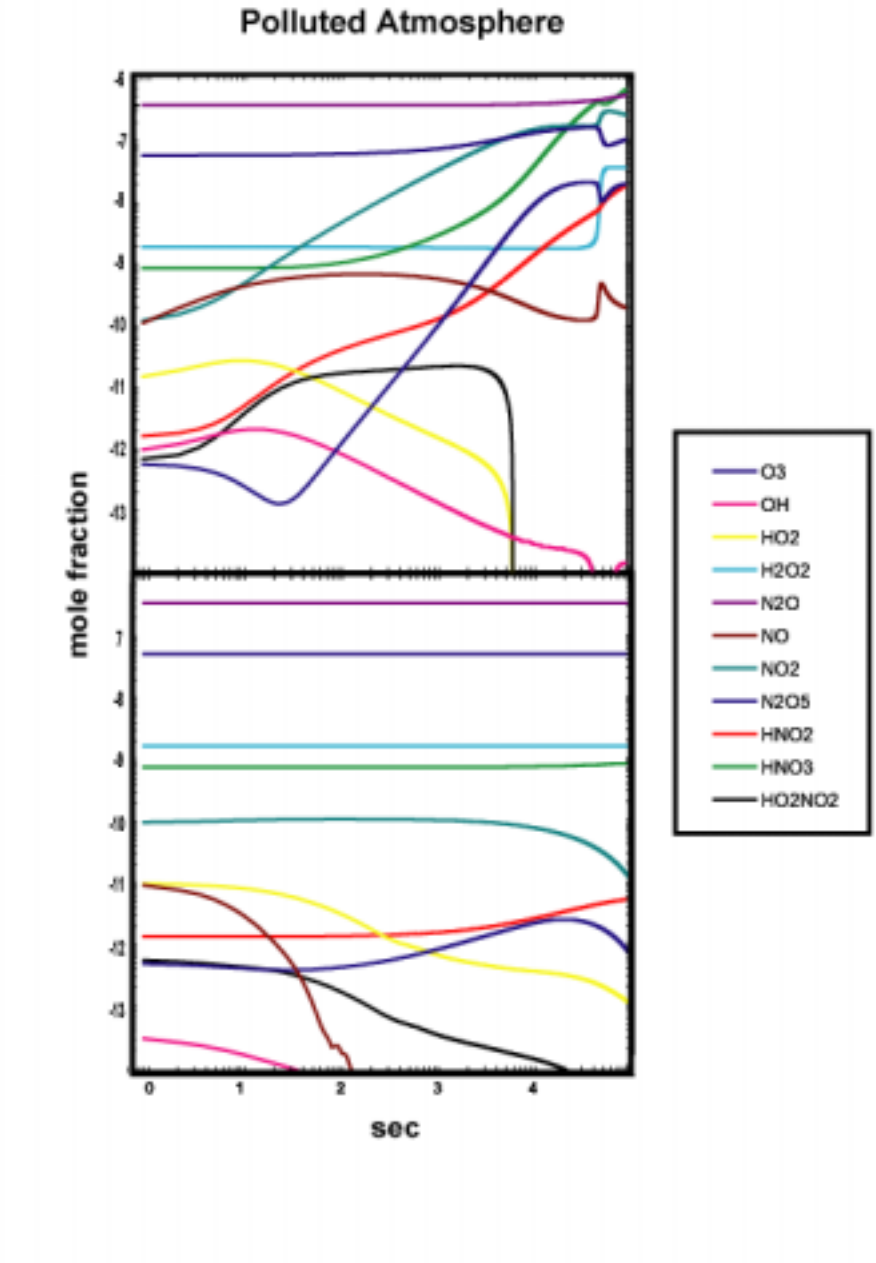

Figure 5. Molecular species concentrations (mole fraction vs. cm) for [a] 0.1 micro Ci, [b] 1.0 micro Ci, and [c] 100 micro Po210 alpha source.

[a]

[b]

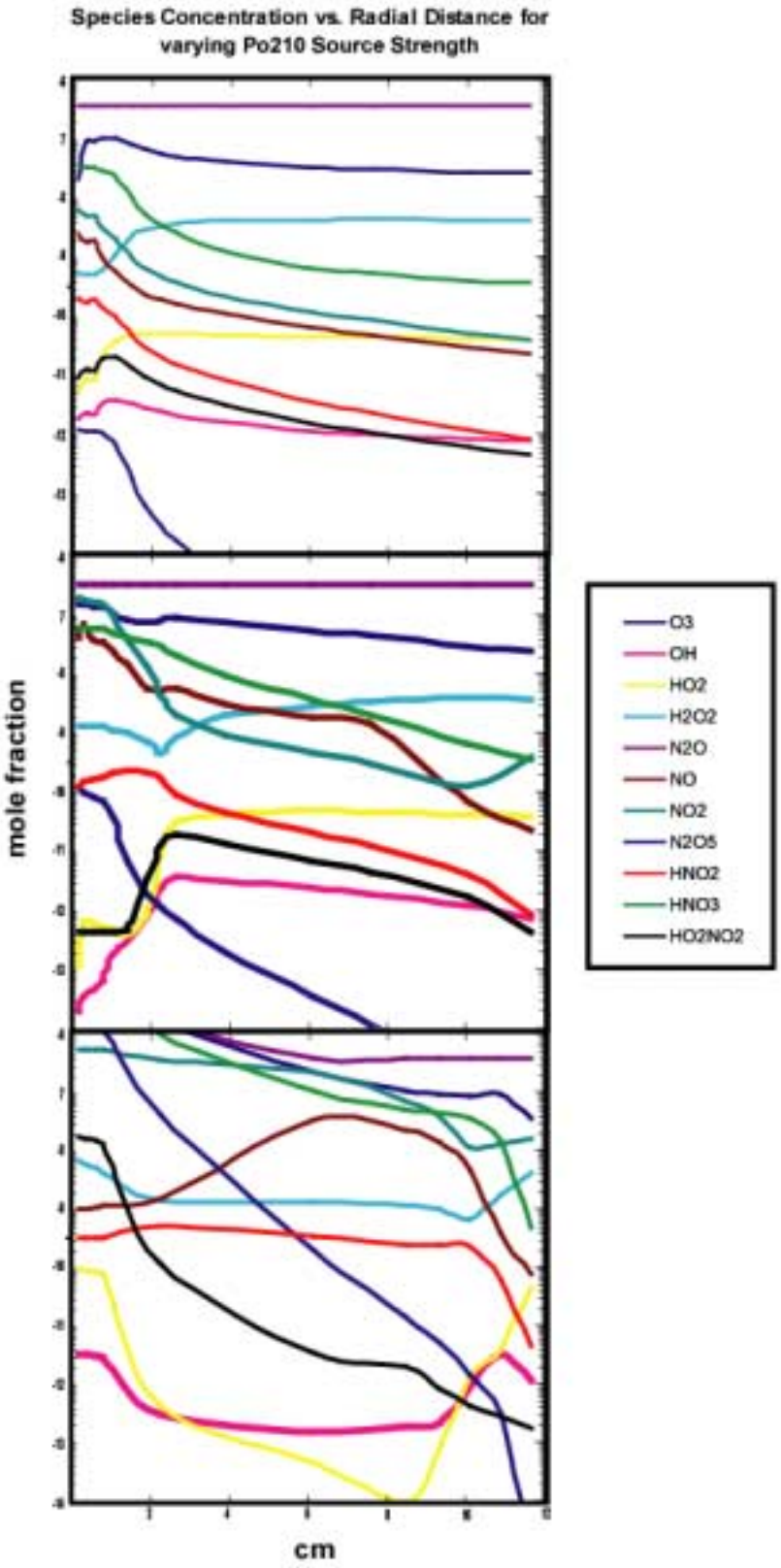

Figure 6. Molecular species concentrations (mole fraction vs. cm) for [a] 0.1 micro Ci, [b] 1.0 micro Ci, and [c] 100 micro Ci Sr90 beta source.

[a]

[b]

[c]